JGR Solid Earth

RESEARCH ARTICLE
10.1029/2023JB027551

Do Subducted Seamounts Act as Weak Asperities?

Sungho Lee[1], **Eunseo Choi**[1], **and Christopher H. Scholz**[2]

[1]Center for Earthquake Research and Information, The University of Memphis, Memphis, TN, USA, [2]Lamont-Doherty Earth Observatory, Columbia University, Palisades, NY, USA

Key Points:

- The founding case for the weak asperity model of seamounts is refuted, thus calling into question the entire hypothesis
- Applying the strong asperity model to the southern Japan trench's subducting seamount provides a source for historical tsunami earthquakes
- The strong asperity model also explains "hang-up" earthquakes propagating from a stationary seamount into the surrounding creeping region

Supporting Information:

Supporting Information may be found in the online version of this article.

Correspondence to:

S. Lee,
slee29@memphis.edu

Citation:

Lee, S., Choi, E., & Scholz, C. H. (2023). Do subducted seamounts act as weak asperities? *Journal of Geophysical Research: Solid Earth*, *128*, e2023JB027551. https://doi.org/10.1029/2023JB027551

Received 26 JUL 2023
Accepted 7 NOV 2023

Author Contributions:

Conceptualization: Sungho Lee, Christopher H. Scholz
Data curation: Sungho Lee
Formal analysis: Sungho Lee, Eunseo Choi, Christopher H. Scholz
Investigation: Sungho Lee, Eunseo Choi, Christopher H. Scholz
Methodology: Sungho Lee
Supervision: Christopher H. Scholz
Visualization: Sungho Lee, Eunseo Choi
Writing – original draft: Sungho Lee, Eunseo Choi, Christopher H. Scholz
Writing – review & editing: Sungho Lee, Eunseo Choi, Christopher H. Scholz

Abstract The additional work of ploughing makes seamounts more resistant to subduction and more strongly coupled than smoother areas. Nevertheless, the idea that subducted seamounts are weakly coupled and slip aseismically has become dominant in the last decade. This idea is primarily based on the claim that a seamount being subducted in the southern Japan Trench behaves this way. The key element in this assertion is that large $M \sim 7$ earthquakes that abut the leading edge of the seamount require that the seamount be aseismically sliding to initiate them. More recent observations show instead that the surrounding region is aseismically sliding while the seamount acts as a stationary buttress. Here we re-examine this case and model it with both weak and strong asperity assumptions. Our modeling results show that only a strong asperity model can produce this type of earthquake. Strong asperities also rupture the seamount in great earthquakes with long recurrence times. This provides the previously unknown source for a series of great tsunami earthquakes that have occurred along the southern Japan Trench, the most recent being the 1677 M8.3–8.6 Enpo Boso-oki tsunami earthquake. The "weak asperity" hypothesis is thus found to be false in this foundational example.

Plain Language Summary This study challenges the widely accepted hypothesis that subducted seamounts act as "weak asperity." Through a comprehensive examination of the case study in the southern Japan Trench, we provide compelling evidence and modeling results that refute this hypothesis and present a new understanding of the seismic mechanisms associated with subducted seamounts. Our research is based on an abundance of new data, meticulous analysis, and advanced modeling techniques. It demonstrates that only steady-state stable sliding occurs in a weak asperity model whereas seamount acts as a stationary buttress, leading to the occurrence of "hang-up earthquakes" in the stable sliding region. This finding not only contradicts the "weak asperity" hypothesis but also provides valuable insights into the recurrence patterns of large-slip events. Based on the modeled slip magnitude and recurrence interval, our work uncovered the previously unidentified source of the significant tsunamis occurring in Japan, opposite the southern Japan Trench.

1. Introduction

A subducting seamount is a prime example of what is known in the friction literature as an asperity: a protrusion on a frictional sliding surface. During sliding an asperity of a harder material will plough a groove through the softer material of the contacting surface. The work done in ploughing the groove increases the frictional resistance force on the asperity (Jaeger & Cook, 1976, p. 55). Seamounts, which are of volcanic origin, similarly often plough through the softer sediments of the accretionary prism when they subduct, leaving furrows back-filled with lower velocity sediments (Bangs et al., 2006; Dominguez et al., 1998; Park et al., 2009; Ranero & von Huene, 2000; Tsuru et al., 2002).

Models of subducting seamounts (Baba et al., 2001; Scholz & Small, 1997; Sun et al., 2020) have elaborated on this basic result. They show that the ploughing force is concentrated on the leading flank of the seamount, where it results in increased normal stress and hence friction. This area is thus likely to be strongly seismically coupled such that it slips in large earthquakes and is locked in the interim. In contrast, the trailing flank is in a stress shadow, where the effective normal stress is low. This area is more likely to be the site of slow earthquake events and tremor.

1.1. The Weak Asperity Hypothesis and Its Refutation

Contrary to these findings, Mochizuki et al. (2008) argued that a seamount being subducted below the southern Japan Trench is weakly coupled with low friction and is slipping aseismically. Wang and Bilek (2011) expanded

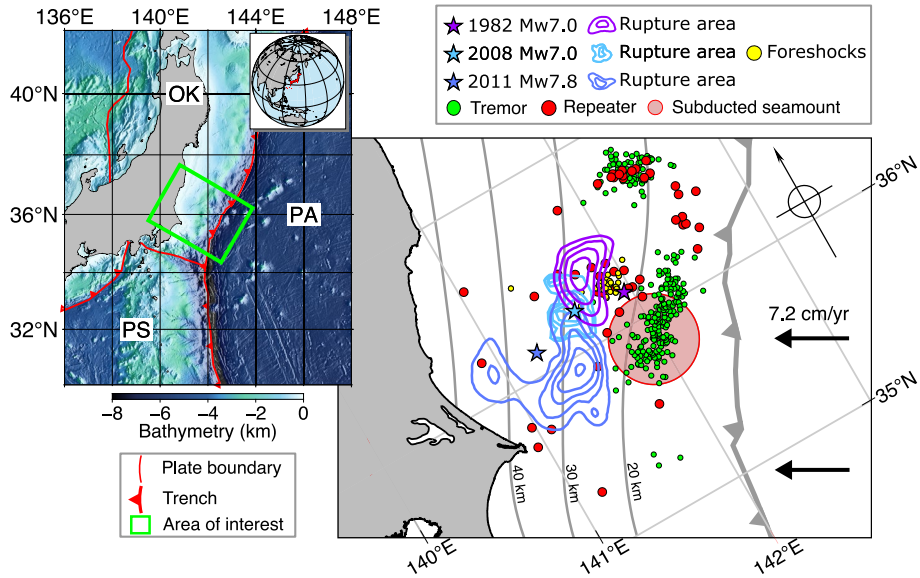

Figure 1. (left) Bathymetry around Japan. The green box is the Ibaraki-oki study area. Red lines with sawtooth symbols represent the subduction boundaries. OK: Okhotsk plate; PA: Pacific plate; PS: Philippine Sea plate. (right) Epicenters and rupture areas of the three Mw≥7.0 events that occurred in Ibaraki Oki (Kubo & Nishikawa, 2020). Purple contours show the 1982 Mw 7.0 rupture area with values increasing inward from 0.4 m at a 0.1 m interval. Sky blue contours show the 2008 Mw 7.0 rupture area with values increasing inward from 0.6 m at a 0.3 m interval. Dark blue contours show the 2011 Mw 7.8 rupture area with values increasing inward from 1.26 m at a 1.26 m interval. Gray lines are the contours of the depths to the top of the Pacific slab from Slab 2.0 (Hayes et al., 2018). The thick gray line with sawtooth symbols is the subduction boundary between OK and PA. The black arrows represent the convergence direction with the convergence rate annotated on top.

on this claim and argued that subducted seamounts predominately subduct aseismically. Because Wang and Bilek's claim is primarily based on Mochizuki et al.'s, we investigate the weak asperity hypothesis by a close examination of that case. This is also one of the most well documented cases, with several new observational studies that postdate the study of Mochizuki et al., bringing new evidence to bear on the controversy. All relevant observations are summarized in Figure 1.

Based on a month-long occupation of a local ocean-bottom seismometer (OBS) network in 2005, Mochizuki et al. noted that the seamount area was devoid of seismicity. They stated that this meant that the seamount was characterized by "either very weak or nearly perfect interplate coupling." They chose the former interpretation because, as will be explained later, they thought it necessary for the seamount to be frictionally weak and thus aseismically slipping for it to initiate M7 earthquakes that occur just down-dip from the seamount.

The context of their paper indicates that by very weak coupling they mean low friction and aseismic slip and by nearly perfect coupling they mean high friction and a locked, seismically coupled, interface. Their interpretation that seismic quiescence indicates aseismic slip is contrary to observations, either elsewhere or in their study area. The so-called "creeping section" of the San Andreas fault, the first place where aseismic slipping was observed, is marked by a high steady rate of low magnitude seismicity, which, though highlighting the presence of the fault, amounts to only a few percent of its moment release rate (Amelung & King, 1997). The same behavior is observed in seismically decoupled subduction zones, such as the Tonga-Kermadec or the Marianas (Scholz & Small, 1997).

A more recent 6 month-long study in 2011 of the area of the subducted seamount with a dense OBS array clarifies and expands on their earlier observations (Yamaya et al., 2022). This study found that interplate thrust earthquakes with slip vectors parallel to the subduction direction occur predominately in the area to the north and northwest of the seamount (Figures 2a and 2b). Many repeater earthquakes occur in this area (Figure 1), which allowed Uchida et al. (2009) to infer that the area around the seamount is aseismically slipping at rates between 1 and 3 cm/yr. This shows that in this area also, aseismic slip is associated with high rates of small magnitude interplate seismicity.

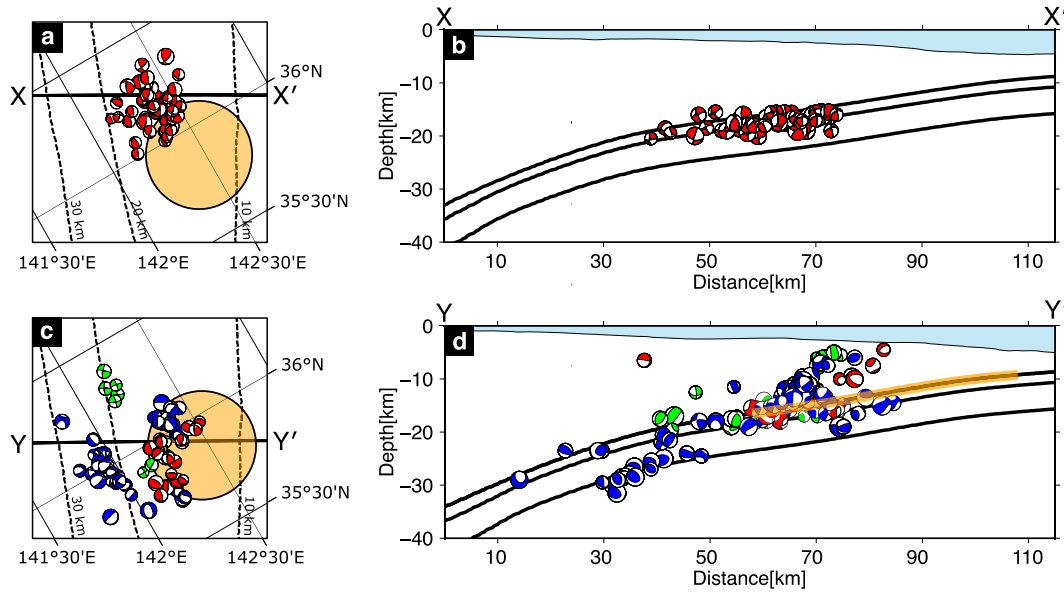

Figure 2. (a) Focal mechanisms of the interplate thrust events from Yamaya et al. (2022). The dashed lines are contours of the depths to the top of the Pacific slab from Japan Integrate Velocity Structure Model Version 1 (Koketsu et al., 2012). The orange circle shows the location and size of the subducted seamount (Mochizuki et al., 2008). X-X' marks the location of the cross-section shown in (b). (b) Cross section along X-X' with the interplate thrust events projected on it. The blue region represents the ocean. From top to bottom, the three black solid lines mark the top of the layer 2, the top of the layer 3, and the Moho of the Pacific slab. (c) The mixed focal mechanisms not directly related to the relative plate motion (Yamaya et al., 2022). Red: reverse; blue: normal; green: strike-slip. (d) Cross-section along Y-Y' with the projected events with mixed focal mechanisms. The thick orange line represents the seamount.

Intraplate earthquake produce a very different pattern. There is a cluster of intraplate earthquakes with a mixture of focal mechanisms that occurs within and above the leading flank of the seamount, indicating localized deformation resulting from ploughing (Figures 2c and 2d). In contrast, and in agreement with Mochizuki et al, Figure 2a shows that very few interplate earthquakes occur on the seamount. Such interplate quiescence is a typical property of the locked zones of both continental faults and subductions zones that are seismically coupled. The absence of interplate earthquakes at the frontal flank of the seamount must likewise indicates that this section of the seamount is locked. The trailing flank, on the other hand, is associated with tremor (Figure 1). This indicates low effective normal stresses there, as expected from models (Hori et al., 2001; Sun et al., 2020).

The relationship between the seamount and large adjacent earthquakes is revealing. The rupture zone of the M_w 7.8 Ibaraki-oki earthquake of 2011 propagated up-dip and stopped at the seamount boundary (Figure 1), suggesting that the latter acted as a barrier (Kubo et al., 2013). This indicates that the seamount must contrast greatly in strength or stress with the surrounding area. There has been a series of $M \sim 7$ earthquakes with rupture areas, as defined by their aftershocks, that abut the down-dip edge of the seamount (Kubo & Nishikawa, 2020) (Figure 1). The epicenter of 1982 event and the foreshocks of the 2008 event occurred closer to the seamount than the main part of their rupture areas (Figure 1), suggesting that the earthquakes propagated away from the seamount. Trying to explain the occurrence of these earthquakes led Mochizuki et al. to their hypothesis that the seamount was sliding aseismically. If the seamount was creeping, they reasoned, stress would accumulate at its down-dip edge, which they proposed would initiate the M7 earthquakes. This is the key assumption behind their 'weak asperity' hypothesis.

The more recent findings render this assumption superfluous. As mentioned above, the areas in the vicinity of the seamount have been found to be aseismically slipping at a rate of 1–3 cm/yr (Uchida et al., 2009), and this provides the convergence on the seamount necessary to generate those M7 earthquakes without requiring the seamount to creep. The idea of Mochizuki et al. that the generation of those earthquakes requires convergence was correct but they were mistaken in the assumption that this was provided by the creeping of the seamount. This led them to infer the wrong properties for the seamount. This was the origin of the 'weak asperity' model. Because these earthquakes seem to result from slip 'hanging up' near the stationary seamount, we call them 'hang-up' earthquakes.

1.2. Hang-Up Versus Repeater Earthquakes

These $M \sim 7$ "hang-up" events down-dip of the seamount recur at roughly 20-year intervals. In this, they resemble repeater events commonly observed on creeping faults (Nadeau et al., 1995), but they differ from that type of earthquake in several important aspects. Repeaters re-rupture precisely the same fault area and with very high stress drops, ~100 MPa (Dreger et al., 2007). They are thus interpreted as re-rupturing the same high strength asperity. The aftershock areas of the last two hang-up earthquakes of 1982 and 2008 abut the seamount (Kubo & Nishikawa, 2020), but their areas of major slip, as seen from their finite source models in Figure 1, are farther down-dip and only partially overlap. The stress drops of these earthquakes were quite low, ~1–3 MPa (Kubo & Nishikawa, 2020). Earlier examples show even more variation (Kubo et al., 2013). For example, the 1960's episode consisted of two smaller events, one of M6.8 in 1961 followed by an M6.7 in 1965. Unlike typical repeaters, these earthquakes do not rupture the asperity (seamount) itself, and their main moment release occurs down-dip from it, in the creeping area. The average slip release rate over the last two hang-up earthquakes was about 2–3 cm/yr, which lies within the range of the convergence rate of 1–3 cm/yr. This is consistent with the seamount being stationary. Thus, the seamount acts as a locked buttress. These hang-up earthquakes have properties consistent with the model of Sammis and Rice (2001) of earthquakes initiated at the boundary between a creeping region and a locked asperity.

2. Modeling of Subducting Seamounts

We developed numerical models for the two possibilities introduced above: A weak-asperity model corresponding to the frictionally weak seamount proposed by Mochizuki et al., and a strong-asperity model. Representing a two-dimensional, trench-perpendicular cross-section of the Japan trench around the latitude of 36°N (Figure 1), our models were constructed based on the global data sets of topography and bathymetry (SRTM15+ from Tozer et al., 2019), slab geometry (Slab2.0 from Hayes et al., 2018) and plate velocity (NUVEL-1A from DeMets et al., 1994, 2010).

We created numerical models using Pylith Version 2.2.2 (Aagaard et al., 2013; Aagaard & Heien, 2019). This open-source finite element code can model ruptures on a fault loaded by kinematic boundary conditions and governed by various friction laws. Listed below are the linear momentum balance equation without body and internal force terms that is solved in our models and the boundary conditions:

$$\nabla \cdot \sigma_{ij} = 0, i, j = x, y, z, \tag{1}$$

$$\sigma_{ij} n_j = T_i \text{ on } S_T, \tag{2}$$

$$u_i = u_i^v \text{ on } S_u, \text{and} \tag{3}$$

$$R_{ki}\left(u_i^+ - u_i^-\right) = d_k \, on \, S_f, \tag{4}$$

where σ_{ij} is the stress tensor (positive for tension), normal vector n_j, traction T on surface S_T, displacement u_i^v on surface S_u, and slip d_k on fault surface S_f. The tractions and fault slip are in global coordinates, and R_{ki} is a rotation matrix that transforms the global coordinate system to the fault coordinate system. PyLith checks for failure at every time step using an inequality based on the friction law "$\tau - \mu_s \sigma_n > 0$" at every time step, where τ is shear stress and σ_n is normal stress. Also, the code calculates stress change and slip as much as the difference of static (μ_s) and dynamic (μ_d) friction coefficients, and then frictional healing from μ_d to μ_s is carried out in subsequent time step.

We took a cross-section cutting through the seamount with dimensions of 1,000 km in length and 250 km in thickness (Figures 1 and 3). Surface topography, bathymetry, and the top interface of the Pacific slab from the open data sources (Hayes et al., 2018; Tozer et al., 2019) were imposed on the geometry of the computational domain. The bottom interface was determined to have a width of 130 km (orange curve in Figure 3). To account for the asperities on the fault interface, specifically the slab top, we incorporated visual observations of bumps made by OBS (station numbers are 20, 8, 22, 23) along the EW exploration line, which corresponds to the position of the seamount mentioned in Mochizuki et al. (2008). These observed bumps were then translated onto the top surface of the slab within our numerical model. The seamount was located at depths of 17 and 23 km, as indicated by the magenta curve in Figure 3. Its width is approximately 30 km, which may be narrower than the estimated

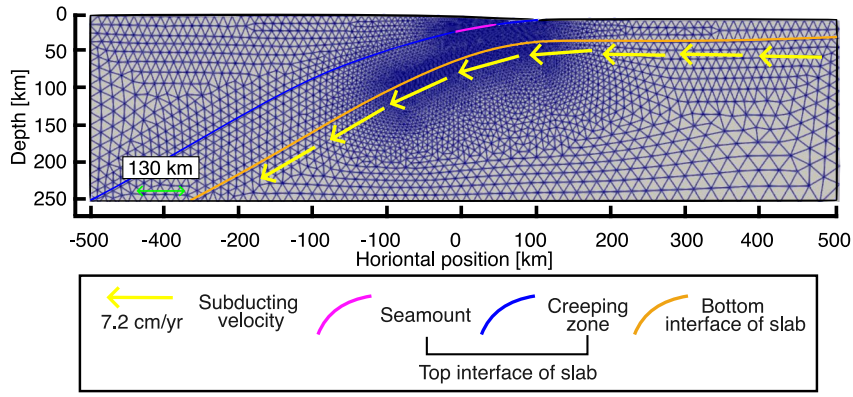

Figure 3. Numerical domain and mesh.

width of 50 km reported by Mochizuki et al.. It is possible that their estimation included buffer or transition areas from velocity-weakening friction to stable sliding regions. However, in our analysis, we solely considered the seamount itself, specifically focusing on the visually observed bumps. After defining the geometry, we discretized the computational domain into a variably sized triangular mesh using Trelis 16.0 (Coreform LLC, n.d.). The mesh was refined near the seamount on both interfaces of the slab (Figure 3).

The subducting rate of the Pacific slab was prescribed to be 7.2 cm/yr on the bottom interface of the slab (DeMets et al., 1994, 2010). The left side was fixed, and the bottom and right sides, except for the slab portion, were set to a roller-boundary condition. The top and right sides of the slab portion were free of constraints.

As the major portion of the numerical model must be composed of peridotite given our domain of interest, we assumed homogeneous peridotite for the entire space for the elastic properties. We assigned a rheology of the linear Maxwell viscoelasticity to the mantle portion excluding the slab and crust (above a depth of 20 km). The model has a viscosity and elastic moduli reflecting the mantle and slab, and we used a viscosity of 7.9×10^{20} Pa sec (Maxwell time of 375 years), Lamé first and second parameters of 82.9 and 66.8 GPa, respectively, corresponding to Vp and Vs values of 8.1 and 4.5 km/s, subsequently, as well as a density of 3,300 kg/m^3.

The static and dynamic friction coefficients of the subduction interface were 0.2 in the stable sliding regime (i.e., $\mu_s = \mu_d = 0.2$) (Sun et al., 2020) but the coefficients for the asperity were varied as specified in the main text. We used a uniform -20 MPa of normal stress (σ_n), but the shear stress (τ) was set to $\mu_d\sigma_n + 0.05$ MPa on the top interface of the slab because we assumed there was an event occurring right before our simulations. This initial condition prevents initial slip at the beginning and adequately reduces time taken for stress to build up until the first rupturing event. Other factors that can modify friction, such as pore fluid pressure, temperature, chemical inhomogeneity, and water-rock reactions are not explicitly considered in this study.

We ran the weak and strong asperity models for 500 and 5,000 years with a time-step size of 5 years, which was also used as the sampling rate for output. The weak asperity model was run for a shorter period of time because it reached a steady-state early on.

3. Results

3.1. Weak Asperity Model

The static and dynamic friction coefficients of the top interface of the subducting slab were both set at 0.2 in the stable sliding region, following Sun et al. (2020). For consistency with the weak asperity model (Mochizuki et al., 2008), the seamount's static and dynamic friction coefficients were both set to be 0.15. Throughout the model duration of 500 years, slip continuously accumulated over the entire subduction interface without any instabilities such as the seamount rupture or hang-up events (Figure 4a). This result suggests that, when a seamount is a weak asperity, slip instabilities such as hang-up earthquakes could not occur and only steady-state stable sliding or creeping could occur. The seamount patch slipped at the rate of 7.56 cm/yr (Figure 4b), which is slightly greater than the loading velocity of 7.2 cm/yr. This behavior originates from the curved geometry and the non-uniform thickness of the slab (Figure S1 in Supporting Information S1).

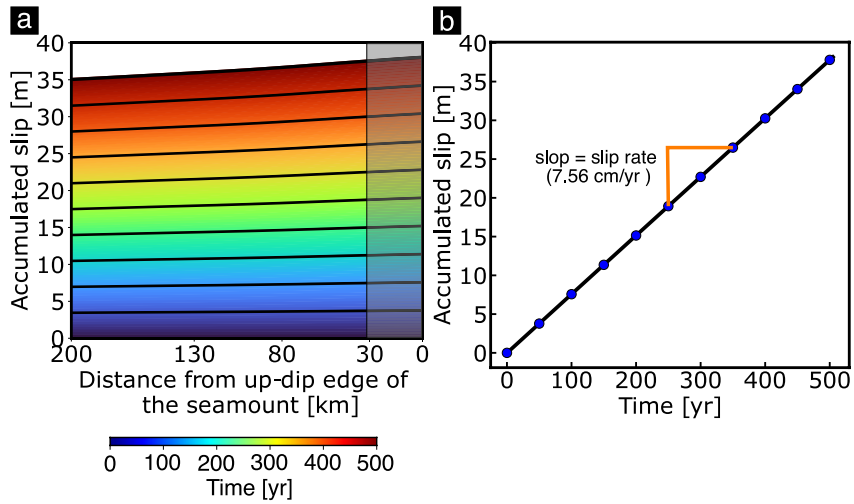

Figure 4. Results of weak asperity model: (a) Accumulated slip along the top interface of the slab as a function of distance from the up-dip edge of the seamount. Black lines are plotted every 50 years and the gray box marks the extent of the seamount. (b) Time history of the accumulated slip at 15 km from up-dip edge of the seamount. Blue dots are drawn at 50 year intervals.

3.2. Strong Asperity Model

The ploughing by a seamount leads to the development of higher normal stresses on the leading flank of the seamount, increasing shear stresses in that region by a factor of 2.5 relative to the average for a seamount with a leading flank slope of 0.10 (Sun et al., 2020) like the one in the southern Japan Trench. Based on this estimation, the seamount as a strong asperity is represented by a static friction coefficient (μ_s) of 0.5 and a dynamic coefficient (μ_d) of 0.2. The stress drop parameter, $\mu_s - \mu_d$, is 0.3.

The time history of the accumulated slip distribution on the subduction interface shows nearly periodic ruptures of 25–27 m slip (Figure 5a). During these seamount-involving ("primary" hereafter) ruptures, the surrounding stable-sliding regions rupture as well (Figure 5a). The regularity of the intervals between the primary ruptures is shown by the slip history at the middle of the seamount (Figure 5b). The mean recurrence interval of these events is 415.5 ± 44.2 years and their mean slip magnitude is 26.6 ± 1.87 m. These values are compatible with those of mega earthquakes in a subduction zone (Satake, 2015). The recurrence intervals and slip magnitudes of the primary rupture events show a linear scaling with the stress drop parameter (Figure 6) but not with the absolute values of friction coefficients. The models with the stress drop parameter of 0.3 exhibited recurrence intervals of 350–450 years and slip magnitudes of 22–32 m. Our preferred value for the friction difference is 0.3 because it agrees with the values for the shear stress on the frontal face of the seamount in the model of Sun et al.

The "interseismic" intervals between two primary ruptures are characterized by stuck periods ("hang-ups") and the "hang-up earthquakes" releasing them. Those hang-up events occur down-dip from the seamount, with various slip magnitudes. In the interval from 2140 to 2565 years (marked on Figure 5b), the down-dip stable-sliding region crept for about 40 years following the previous primary rupture while the seamount remained locked as represented by the regularly spaced blue curves in Figure 5c. Then, the whole subduction interface including the stable sliding region became stuck for about 140 years (the first orange curve above the blue curves in Figure 5c). This was followed by a hang-up earthquake which ruptured the down-dip stable region and the near-edge portion of the seamount. The ruptured region and slip distribution is represented by the green bars bounded by the first and second orange curves from the bottom in Figure 5c. The hang-up earthquake was immediately followed by another hang-up of a 100-year duration. A few cycles of hang-ups and hang-up earthquakes were repeated with variable slip amounts and durations. The ruptured area penetrated ever deeper into the seamount patch (Figure 5c) until eventually another primary rupture occurred. The hang-up cycles during this interseismic interval are well illustrated by the slip history at a location 50 km down dip from the deeper end of the seamount patch (Figure 5d). The same overall behaviors were observed in all the other interseismic periods (Figure S2 in Supporting Information S1) although the number, slip amount, and timing of the hang-up earthquakes slightly varied.

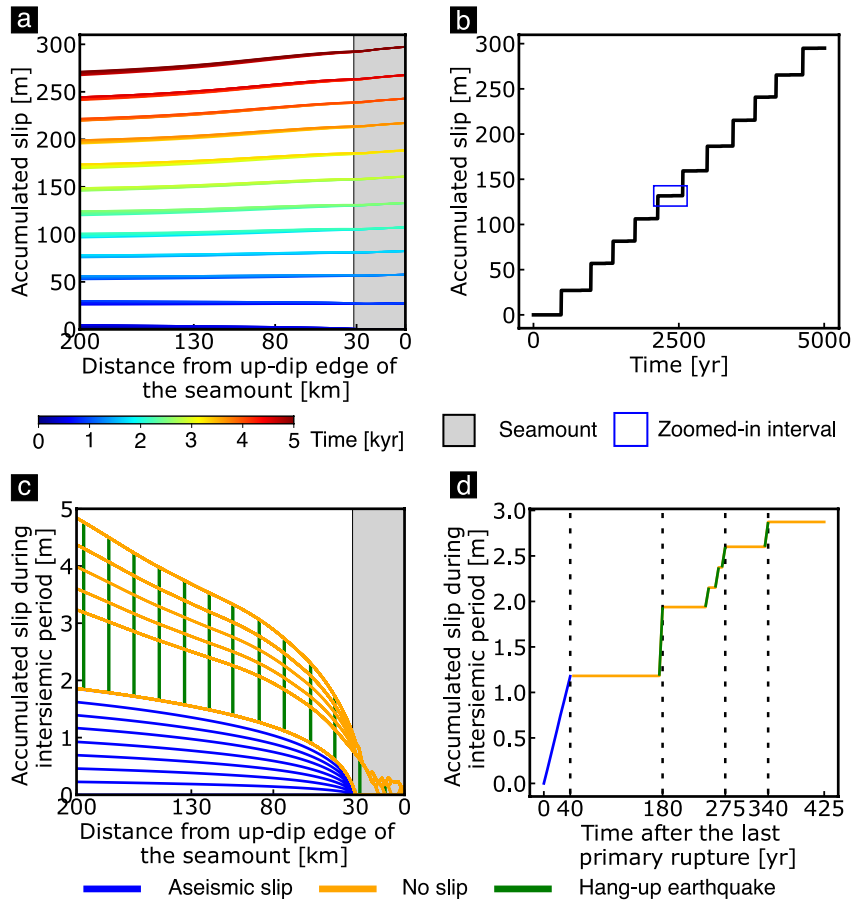

Figure 5. Results of strong asperity model: (a) The accumulated slip along the top interface of the slab. (b) The time history of accumulated slip at the middle of the seamount. The mean slip magnitude and mean recurrence interval were 28 m and 462 years, respectively. (c) The accumulated slip at 5-year intervals along the top interface of the slab during the interseismic period from 2140 to 2565 years. (d) The temporal change in accumulated slip at 50 km down-dip from the down-dip edge of the seamount.

3.3. Hang-Up Earthquake Mechanism

The mechanism for a hang-up earthquake can be illustrated with a simple kinematic model (Figure 7a). The seamount is locked and acts as a buttress against both the creep of the down-dip stable-sliding region and the rupture by a hang-up earthquake. The brittle-ductile transition (BDT) occurs at the distance, B, from the leading edge of the seamount (i.e., at $x = B$ in Figure 7a) constraining the amount of dynamic rupture. The amount of stable slip goes to zero as the seamount is approached ($x \rightarrow 0$) over the distance R (Figure 7a). R is a characteristic dimension that depends on the size of the seamount. In the region, the $R < x < B$, slip (u) accumulates almost uniformly at a constant rate as $u = vt$ during the down-dip creeping period following the previous primary rupture as depicted by the slip profiles u_1 *to* u_m for $t = t_1$ to t_m in Figure 7a. During the down-dip creeping period, a stress concentration builds up at the leading edge of the seamount, as shown by the orange-dotted curve in Figure 7b. When the down-dip region locks up, the slip distribution profiles do not change until $t = t_n$, and stress builds up on the entire slab interface as shown as the green-dotted curve in Figure 7b. When the hang-up is released in a dynamic rupture event, the displacement profile jumps from u_n ($=u_m$) to u_{n+1} (Figure 7a). As shown by the red curve in Figure 7b, this relaxes the stress concentration on the leading edge of the seamount where slip occurred and the stress concentration migrates inwards. The hatched area in Figure 7a indicates the slip that occurred during the hang-up earthquake. According to the finite source models (Figure 1), the radius of the main slip area in the hang-up event, denoted as $r(fsm)$ in Figure 7a and is located some distance down dip from the seamount. In contrast, the radius defined by aftershocks, denoted as $r(a)$, extends to the seamount.

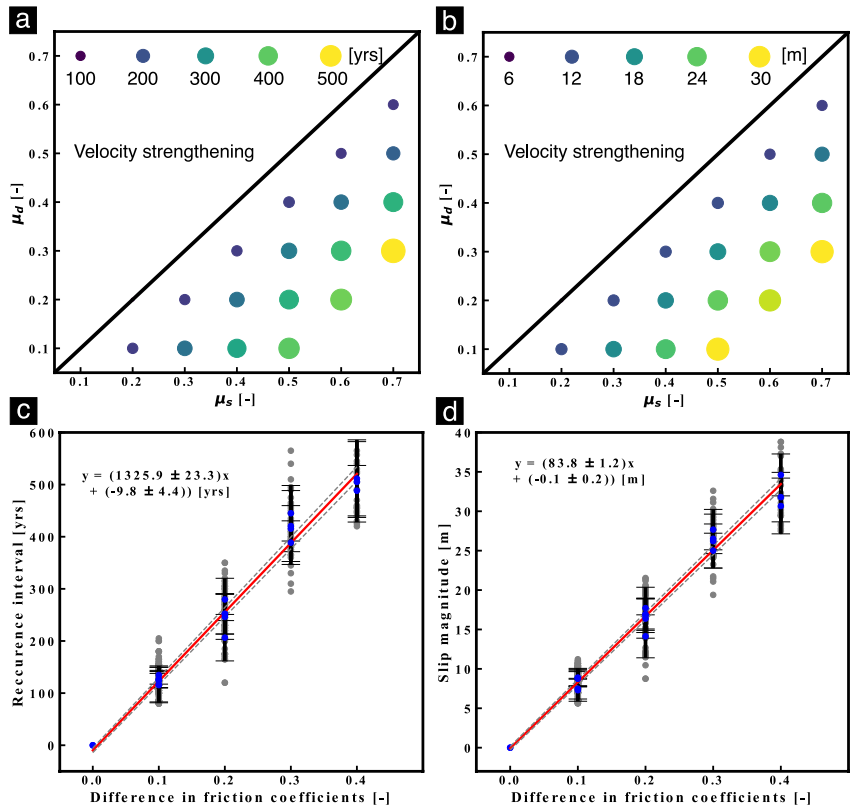

Figure 6. (a) Mean recurrence time and (b) mean slip magnitude with various combinations of μ_s and μ_d. (c) Recurrence time and (d) slip magnitude with stress drop parameter ($\mu_s - \mu_d$).

Slip due to a hang-up event continuously increases with depth in our numerical model (Figure 5c). This is because our model does not implement a BDT that would constrain slip at depth. For example, in the study area (Figure 1), seismic slip is known to be limited to depths shallower than 50 km (Igarashi et al., 2001; Uchida et al., 2009). However, to include such a BDT zone would entail introducing a viscous-plastic rheology at those depths, which is beyond the scope of this investigation. Instead of explicitly considering a viscous-plastic rheology, we can evaluate the effect of a BDT constraining slip by introducing approximate velocity-strengthening effects below an assumed BDT depth of 50 km. The models with $\mu_d = 0.4$ or 0.45 (cf. $\mu_s = 0.2$) below the BDT depth demonstrate that the area of the largest slip can be confined in the area between the seamount and the BDT depth (Figure 8). This explains how the hang-up events could be driven by the seamount yet seem to remain physically distant from it. Thus, the seamount acts as a stuck, strong barrier even though a portion of it may experience slip during a hang-up event shown as in Figure 5c.

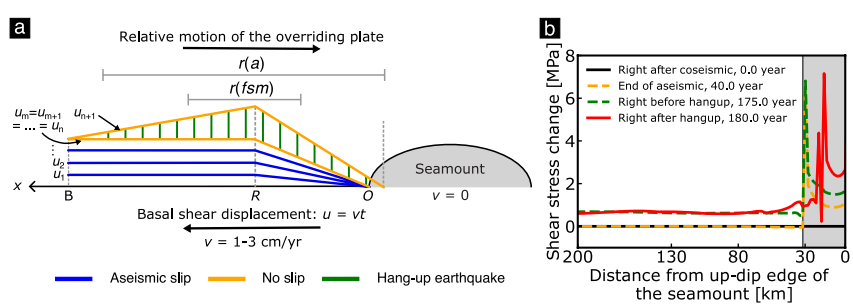

Figure 7. (a) Illustration of a simplified kinematic model depicting the hang-up mechanism. Please refer to the accompanying text for a detailed explanation. (b) Shear stress change obtained from our numerical model along the top interface of the slab at four-times during the hang-up cycle. Shear stress change is defined as the difference between the shear stress immediately following the last primary stick-slip event and the current shear stress.

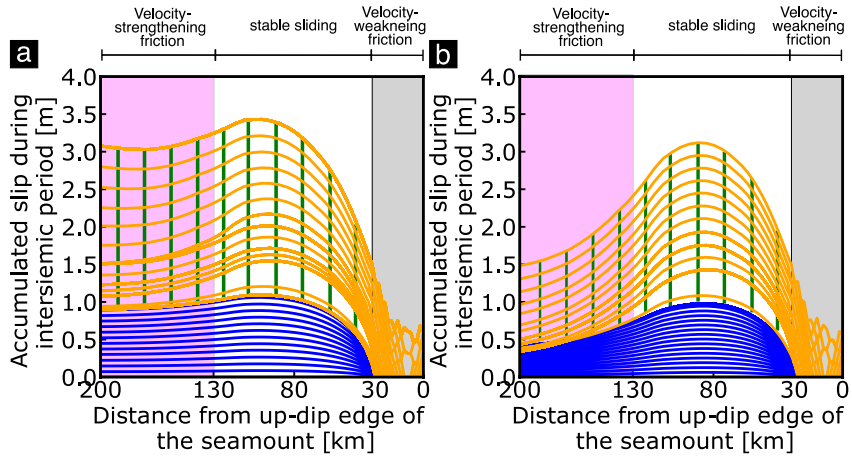

Figure 8. The accumulated slip along the top interface of the slab during an interseismic period. The reference model was modified with (a) 0.4 and (b) 0.45 of dynamic friction coefficient (μ_d) below the depth of 50 km, which is corresponding to 130 km away from the up-dip edge of the seamount.

The data in Figures 2c and 2d demonstrates the intense fracturing that accompanies the ploughing deformation above the frontal flank of the seamount. This validates the model results of Dominguez et al. (1998). These fractures could provide a pathway for fluid expulsion and hence lead to a reduction of pore pressure at the seamount and hence further enhance its frictional coupling (Dominguez et al., 2000; Madden et al., 2022). While our numerical model has limitations when it comes to quantifying fluid pressure, the outcomes are anticipated to align with models that consider pore fluid effects and the intense deformation in the upper plate.

The subduction plate interface exhibits stable frictional sliding at a rate slower than the overall plate motion. This slower movement will result in stress gradually increasing over time. This phenomenon is known as partial coupling of the subduction interface. The long-term nature of the partial coupling of the subduction interface observed by Uchida et al. and others remains uncertain. If this partial coupling is indeed a persistent phenomenon, it poses significant challenges for modeling the subduction process. It would imply a temporal stress buildup throughout the entire earthquake cycle, which contradicts the assumption of steady-state stable sliding at a constant friction value. However, addressing this issue falls outside the scope of our work, and therefore we have not included the partial coupling in our subduction model. As a result, our model does not capture the current periodic behavior of the hang-up events. It is important to note that our objective was not to develop a predictive model for these events but rather to demonstrate that they can only occur when strong, locked asperities are present, as opposed to weak, creeping asperities.

4. Discussion

4.1. Tsunami Earthquakes Associated With the Rupture of the Subducted Seamount

There is a history of tsunamis that have inundated the coastline opposite the southern Japan Trench as indicated by the blue shaded areas in Figure 9. The Enpo Boso-oki tsunami earthquake of 1677 is historically documented. Earlier events are known from tsunami deposits along the Ibaraki coast from Juo to the Boso Peninsula in Chiba. They are particularly well developed in Choshi. These deposits document two earlier tsunami earthquakes, one within the period 896–1445 CE and one in the time range 488 CE–215 BCE for example, Higaki et al. (2021). Various models of the source area of the 1677 earthquake show it extending from the area of the subducted seamount to as far as 150 km to the south (Yanagisawa et al., 2016), as shown in Figure 9. Yanagisawa et al. (2016) modeled the observations of the tsunami effects and concluded that the 1677 earthquake was in the range M8.3–8.6 with a slip of 11–16 m. Pilarczyk et al. (2021) modeled the tsunami deposits from the 896–1445 CE event, and assuming the same source area as the 1677 event, concluded that it had a slip of 25 m and a magnitude of 8.8.

The seismic activity along the Japan Trench south of the subducted seamount is typified by spontaneous slow slip events (Nishikawa et al., 2019). These are in the magnitude range 6–6.5 and occur a few times a year

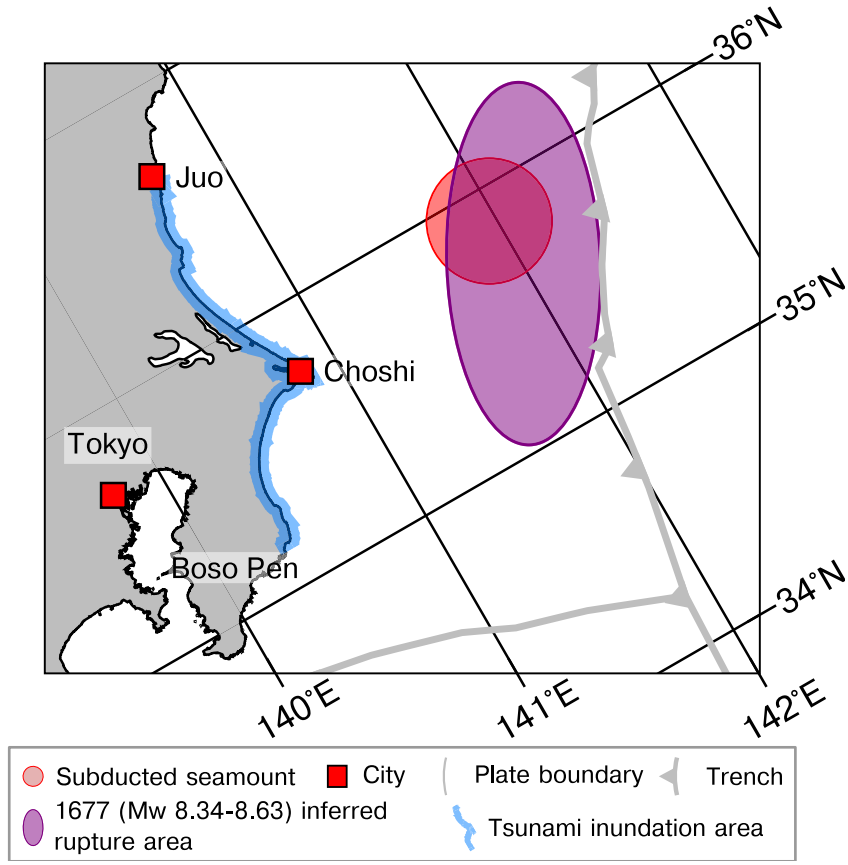

Figure 9. The inferred rupture area of the 1677 M8 earthquake (Higaki et al., 2021) and the tsunami inundation area (Takeuchi et al., 2007).

(Nishimura, 2021). Such shallow SSEs are associated with high pore pressures and low effective stresses (Saffer & Wallace, 2015). This is consistent with other indications (Uchida et al., 2009) that this is an area of low interplate coupling and thus incapable of initiating great earthquakes. Prior to our study, this presented a conundrum: there were no known plausible sources for generating these great tsunami earthquakes. Our finding that the subducted seamount is strongly coupled and ruptures in large slip events with long recurrence times provides the answer to this puzzle. As demonstrated by Duan (2012) and Meng and Duan (2022), such a large energetic slip event at the seamount could propagate for a considerable distance to the south, triggering substantial slip there, as suggested by the proposed tsunami source areas. The rupture of the subducted seamount thus provides the most plausible source for these great tsunami earthquakes.

4.2. Sources of Confusion Regarding the Behavior of Subducted Seamounts

The literature on subducted seamounts exhibits several sources of confusion that have led to some misunderstandings of their behavior. One source comes from the terminology asperity and barrier. The term asperity has different meanings in tribology and seismology. To avoid confusion between them in our discussion here we use boldface for the tribological usage: **asperity**; and italics for the seismological usage: *asperity*. Another seismological term which has no counterpart in tribology is *barrier*. There are two types of barriers which also may lead to confusion.

Asperities are protrusions on frictional surfaces. *Asperities* are regions of unusually large slip within earthquake ruptures. *Barriers* are regions where earthquakes have been impeded or stopped. Subducted seamounts are prime examples of **asperities**.

An **asperity**, simply in consequence of its geometry, will be subject to a higher normal stress than smoother regions. It will therefore have a higher local frictional strength. Within an overall seismically coupled region the

response of an **asperity** to earthquake rupture will depend on the ratio of its initial applied stress to its strength. If this ratio is high enough such that the **asperity** ruptures during the earthquake, it will produce a larger stress drop and hence greater slip than the surrounding regions. Thus, in this case it acts as an *asperity*. Because of its greater stress drop, the **asperity** will have a longer loading cycle than the surrounding regions, hence its seismic cycle will be out of phase with that of its surroundings. This insures that in some other earthquake the **asperity** will be at an early phase of its seismic cycle so that it's stress to strength ratio is low. In this case, it may resist rupturing because of its strength, thus behaving as a *high strength barrier*. Thus, in a seismically coupled region an **asperity** can act as either an *asperity* or a *barrier*. This distinction was explained by Das and Watts (2009) and Bilek and Engdahl (2007) gave an example of each type. Note that in both cases the **asperity** is strong—the difference in behavior results from different stress levels.

Within an overall seismically decoupled region, an **asperity** will be a seismically coupled area isolated within an area that is aseismically slipping. In this case, the **asperity** will always rupture as an isolated *asperity*. That seamounts always act as *asperities* in this case has been pointed out by Scholz and Small (1997) and Bilek and Engdahl (2007).

A *low strength barrier*, on the other hand, is a permanent feature resulting from the presence of weak, frictionally stable material. This is possible under conditions of very low effective normal stresses or the presence of velocity-strengthening material. The two types of barriers are sometimes confused. Wang and Bilek (2011), for example, seem to have confused low strength barriers with high strength barriers in associating the barrier behavior of subducted seamounts with supposed aseismic subduction.

The deformation in the upper plate produced by subducted seamounts often leads to the close juxtaposition of strongly and weakly coupled areas. One needs to be careful in distinguishing these behaviors. As we have shown in the case of the southern Japan Trench seamount, the frontal flank of the seamount is very strongly coupled while the trailing flank is weakly coupled and associated with tremor. The presence of this tremor led Kubo and Nishikawa (Kubo & Nishikawa, 2020) to conclude that the seamount had behaved as a "soft" (low strength) rather than high strength barrier to the 2011 Ibaraki-oki earthquake.

Yokota et al. (2016) are often cited as providing direct geodetic evidence for the coincidence of seamounts with low coupling. The seamount in question, off the Muroto Peninsula of Shikoku (Kodaira et al., 2000) is much smaller than the region of low coupling that it partially lies within, so that it is not possible for the seamount itself to be responsible for the low coupling in the way supposed by Wang and Bilek, as suggested by for example, Todd et al. (2018). That broad low coupling region, that extends between Shikoku and the Kii Peninsula, probably results from the downwarp in the subduction interface in that region (Yamamoto et al., 2017) and has nothing to do with the seamount. This seamount has instead been proposed to have acted as a strong barrier in the 1946 Nankaido earthquake (Kodaira et al., 2000). These interpretations are compatible because the leading flank of the seamount, which is the part expected to be highly coupled (Hori et al., 2001), lies within the highly coupled area as defined by Yokota et al.

In the case of the generally seismically decoupled northern part of the Hikurangi margin of New Zealand, SSEs and tremor are observed down-dip of two smallish subducted seamounts (Wallace & Beavan, 2010; Wallace et al., 2016). There, the ploughing of the seamounts has driven a wedge of subducted sediments below the sedimentary prism where very high pore pressures have developed that host the SSEs (Bell et al., 2010; Ellis et al., 2015). High pore pressures and slow slip also occur in the back-filled furrows trailing the seamounts (Bangs et al., 2006). Although the region as a whole can be considered to have low coupling (Saffer & Wallace, 2015), the seamounts themselves are seismically coupled, having produced a pair of M ~ 7 tsunami earthquakes in 1947 (Bell et al., 2014).

5. Conclusions

Mochizuki et al. (2008) proposed the weak asperity hypothesis as a way of explaining what we now call the "hang-up" earthquakes. They recognized that those earthquakes must occur as a reaction to local convergence. They chose to assume that the region of the hang-up earthquakes was stationary and that the convergence was produced by the seamount, which must therefore be sliding stably and thus be frictionally weak. More recent observations, from the interpretation of repeater earthquakes in the region of the hang-ups, show that just the

opposite is occurring. The hang-up region is converging aseismically and the seamount is stationary. This observation, of a stuck seamount, is consistent with the strong asperity theory of seamounts.

In our modeling of the weak asperity hypothesis we found that a stably sliding region imbedded within another stably sliding region cannot produce a slip instability. In that case, all regions slide stably at all times. In our model with a strong asperity we found that a frictionally locked region can induce a slip instability in an adjacent otherwise stably sliding region in accordance with the analytical solution of Sammis and Rice (2001). This behavior explains hang-up earthquakes.

The strong asperity model also predicts great earthquakes with long recurrence times when the seamount, together with its surrounding region, ruptures. The historic and paleoseismic record shows that great tsunami earthquakes do recur in this area with such long recurrence times. The evidence indicates that the only plausible source region for the initiation of such earthquakes is the subducted seamount of our study.

The weak asperity model thus fails in two ways. It does not provide a means to produce hang-up earthquakes and it does not predict the occurrence of the great tsunami earthquakes that occur along the southern Japan Trench. The strong asperity model predicts both.

Conflict of Interest

The authors declare no conflicts of interest relevant to this study.

Data Availability Statement

All the data in Figures 1, 2, and 9 used in this study have been published by other researchers as referenced in this paper. Pylith's input data for this study are available on Figshare (Lee et al., 2023). PyLith v.2.2.2 is freely available online (Aagaard & Heien, 2019).

Acknowledgments
We thank the Computational Infrastructure for Geodynamics for providing Pylith for this study. We also thank Dr. Alice-Agnes Gabriel, the associate editor, an anonymous reviewer, and Dr. Stephane Dominguez for their constructive comments and suggestions that helped improve our manuscript. This material is based upon wrok supported by the National Science Foundation under Grant 2104002. EC and SL were partially supported by KIGAM (Korea Institute of Geoscience and Mineral Resources).

References

Aagaard, B., & Heien, E. (2019). PyLith (version v2.2.2) [Software]. Computational Infrastructure for Geodynamics. https://doi.org/10.5281/zenodo.3266413

Aagaard, B. T., Knepley, M. G., & Williams, C. A. (2013). A domain decomposition approach to implementing fault slip in finite-element models of quasi-static and dynamic crustal deformation. *Journal of Geophysical Research: Solid Earth*, *118*(6), 3059–3079. https://doi.org/10.1002/jgrb.50217

Amelung, F., & King, G. (1997). Earthquake scaling laws for creeping and non-creeping faults. *Geophysical Research Letters*, *24*(5), 507–510. https://doi.org/10.1029/97GL00287

Baba, T., Hori, T., Hirano, S., Cummins, P. R., Park, J.-O., Kameyama, M., & Kaneda, Y. (2001). Deformation of a seamount subducting beneath an accretionary prism: Constraints from numerical simulation. *Geophysical Research Letters*, *28*(9), 1827–1830. https://doi.org/10.1029/2000GL012266

Bangs, N. L. B., Gulick, S. P. S., & Shipley, T. H. (2006). Seamount subduction erosion in the Nankai Trough and its potential impact on the seismogenic zone. *Geology*, *34*(8), 701–704. https://doi.org/10.1130/G22451.1

Bell, R., Holden, C., Power, W., Wang, X., & Downes, G. (2014). Hikurangi margin tsunami earthquake generated by slow seismic rupture over a subducted seamount. *Earth and Planetary Science Letters*, *397*, 1–9. https://doi.org/10.1016/j.epsl.2014.04.005

Bell, R., Sutherland, R., Barker, D. H. N., Henrys, S., Bannister, S., Wallace, L., & Beavan, J. (2010). Seismic reflection character of the Hikurangi subduction interface, New Zealand, in the region of repeated Gisborne slow slip events. *Geophysical Journal International*, *180*(1), 34–48. https://doi.org/10.1111/j.1365-246X.2009.04401.x

Bilek, S. L., & Engdahl, E. R. (2007). Rupture characterization and aftershock relocations for the 1994 and 2006 tsunami earthquakes in the Java subduction zone. *Geophysical Research Letters*, *34*(20), L20311. https://doi.org/10.1029/2007GL031357

Coreform LLC. (n.d.). *Trelis (version 16.0)*. Coreform LLC. Retrieved from https://coreform.com/products/downloads/

Das, S., & Watts, A. B. (2009). Effect of subducting seafloor topography on the rupture characteristics of great subduction zone earthquakes. In S. Lallemand & F. Funiciello (Eds.), *Subduction zone Geodynamics* (pp. 103–118). Springer. https://doi.org/10.1007/978-3-540-87974-9_6

DeMets, C., Gordon, R. G., & Argus, D. F. (2010). Geologically current plate motions. *Geophysical Journal International*, *181*(1), 1–80. https://doi.org/10.1111/j.1365-246X.2009.04491.x

DeMets, C., Gordon, R. G., Argus, D. F., & Stein, S. (1994). Effect of recent revisions to the geomagnetic reversal time scale on estimates of current plate motions. *Geophysical Research Letters*, *21*(20), 2191–2194. https://doi.org/10.1029/94GL02118

Dominguez, S., Lallemand, S. E., Malavieille, J., & von Huene, R. (1998). Upper plate deformation associated with seamount subduction. *Tectonophysics*, *293*(3–4), 207–224. https://doi.org/10.1016/s0040-1951(98)00086-9

Dominguez, S., Malavieille, J., & Lallemand, S. E. (2000). Deformation of accretionary wedges in response to seamount subduction: Insights from sandbox experiments. *Tectonics*, *19*(1), 182–196. https://doi.org/10.1029/1999TC900055

Dreger, D., Nadeau, R. M., & Chung, A. (2007). Repeating earthquake finite source models: Strong asperities revealed on the San Andreas Fault. *Geophysical Research Letters*, *34*(23), L23302. https://doi.org/10.1029/2007GL031353

Duan, B. (2012). Dynamic rupture of the 2011 Mw 9.0 Tohoku-Oki earthquake: Roles of a possible subducting seamount. *Journal of Geophysical Research*, *117*(B5), B05311. https://doi.org/10.1029/2011JB009124

Ellis, S., Fagereng, Å., Barker, D., Henrys, S., Saffer, D., Wallace, L., et al. (2015). Fluid budgets along the northern Hikurangi subduction margin, New Zealand: The effect of a subducting seamount on fluid pressure. *Geophysical Journal International*, *202*(1), 277–297. https://doi.org/10.1093/gji/ggv127

Hayes, G. P., Moore, G. L., Portner, D. E., Hearne, M., Flamme, H., Furtney, M., & Smoczyk, G. M. (2018). Slab2, a comprehensive subduction zone geometry model. *Science*, *362*(6410), 58–61. https://doi.org/10.1126/science.aat4723

Higaki, H., Goto, K., Yanagisawa, H., Sugawara, D., & Ishizawa, T. (2021). Three thousand year paleo-tsunami history of the southern part of the Japan Trench. *Progress in Earth and Planetary Science*, *8*(1), 28. https://doi.org/10.1186/s40645-021-00415-w

Hori, T., Baba, T., Cummins, P. R., & Kaneda, Y. (2001). Effects of subducted seamounts on the source process of the 1946 Nankai earthquake, SW Japan. In *2nd ACES Workshop Proceedings* (pp. 271–274).

Igarashi, T., Matsuzawa, T., Umino, N., & Hasegawa, A. (2001). Spatial distribution of focal mechanisms for interplate and intraplate earthquakes associated with the subducting Pacific plate beneath the northeastern Japan arc: A triple-planed deep seismic zone. *Journal of Geophysical Research*, *106*(B2), 2177–2191. https://doi.org/10.1029/2000JB900386

Jaeger, J. C., & Cook, N. G. W. (1976). *Fundamentals of rock mechanics* (2d ed., p. 55). Chapman and Hall.

Kodaira, S., Takahashi, N., Nakanishi, A., Miura, S., & Kaneda, Y. (2000). Subducted seamount imaged in the rupture zone of the 1946 Nankaido earthquake. *Science*, *289*(5476), 104–106. https://doi.org/10.1126/science.289.5476.104

Koketsu, K., Miyake, H., & Suzuki, H. (2012). Japan integrated velocity structure model version 1. In *Proceedings of The 15th World Conference on Earthquake Engineering* (Vol. 1, p. 4).

Kubo, H., Asano, K., & Iwata, T. (2013). Source-rupture process of the 2011 Ibaraki-oki, Japan, earthquake (Mw 7.9) estimated from the joint inversion of strong-motion and GPS data: Relationship with seamount and Philippine Sea plate. *Geophysical Research Letters*, *40*(12), 3003–3007. https://doi.org/10.1002/grl.50558

Kubo, H., & Nishikawa, T. (2020). Relationship of preseismic, coseismic, and postseismic fault ruptures of two large interplate aftershocks of the 2011 Tohoku earthquake with slow-earthquake activity. *Scientific Reports*, *10*(1), 12044. https://doi.org/10.1038/s41598-020-68692-x

Lee, S., Choi, E., & Scholz, C. H. (2023). Do subudcted seamount act as weak asperities? [Dataset]. Figshare. https://doi.org/10.6084/m9.figshare.23706156.v1

Madden, E. H., Ulrich, T., & Gabriel, A.-A. (2022). The state of pore fluid pressure and 3-D megathrust earthquake dynamics. *Journal of Geophysical Research: Solid Earth*, *127*(4), e2021JB023382. https://doi.org/10.1029/2021JB023382

Meng, Q., & Duan, B. (2022). Dynamic modeling of interactions between shallow slow-slip events and subduction earthquakes. *Seismological Research Letters*, *94*(1), 206–216. https://doi.org/10.1785/0220220138

Mochizuki, K., Yamada, T., Shinohara, M., Yamanaka, Y., & Kanazawa, T. (2008). Weak interplate coupling by seamounts and repeating M∼7 earthquakes. *Science*, *321*(5893), 1194–1197. https://doi.org/10.1126/science.1160250

Nadeau, R. M., Foxall, W., & McEvilly, T. V. (1995). Clustering and periodic recurrence of microearthquakes on the San Andreas fault at Parkfield, California. *Science*, *267*(5197), 503–507. https://doi.org/10.1126/science.267.5197.503

Nishikawa, T., Matsuzawa, T., Ohta, K., Uchida, N., Nishimura, T., & Ide, S. (2019). The slow earthquake spectrum in the Japan Trench illuminated by the S-net seafloor observatories. *Science*, *365*(6455), 808–813. https://doi.org/10.1126/science.aax5618

Nishimura, T. (2021). Slow slip events in the Kanto and Tokai regions of Central Japan Detected using global Navigation satellite system data during 1994–2020. *Geochemistry, Geophysics, Geosystems*, *22*(2), e2020GC009329. https://doi.org/10.1029/2020GC009329

Park, J.-O., Hori, T., & Kaneda, Y. (2009). Seismotectonic implications of the Kyushu-Palau ridge subducting beneath the westernmost Nankai forearc. *Earth Planets and Space*, *61*(8), 1013–1018. https://doi.org/10.1186/BF03352951

Pilarczyk, J. E., Sawai, Y., Namegaya, Y., Tamura, T., Tanigawa, K., Matsumoto, D., et al. (2021). A further source of Tokyo earthquakes and Pacific Ocean tsunamis. *Nature Geoscience*, *14*(10), 796–800. https://doi.org/10.1038/s41561-021-00812-2

Ranero, C. R., & von Huene, R. (2000). Subduction erosion along the Middle America convergent margin. *Nature*, *404*(6779), 748–752. https://doi.org/10.1038/35008046

Saffer, D. M., & Wallace, L. M. (2015). The frictional, hydrologic, metamorphic and thermal habitat of shallow slow earthquakes. *Nature Geoscience*, *8*(8), 594–600. https://doi.org/10.1038/ngeo2490

Sammis, C. G., & Rice, J. R. (2001). Repeating earthquakes as low-stress-drop events at a border between locked and creeping fault Patches. *Bulletin of the Seismological Society of America*, *91*(3), 532–537. https://doi.org/10.1785/0120000075

Satake, K. (2015). Geological and historical evidence of irregular recurrent earthquakes in Japan. *Philosophical Transactions of the Royal Society A: Mathematical, Physical & Engineering Sciences*, *373*(2053), 20140375. https://doi.org/10.1098/rsta.2014.0375

Scholz, C. H., & Small, C. (1997). The effect of seamount subduction on seismic coupling. *Geology*, *25*(6), 487–490. https://doi.org/10.1130/0091-7613(1997)025<0487:TEOSSO>2.3.CO;2

Sun, T., Saffer, D., & Ellis, S. (2020). Mechanical and hydrological effects of seamount subduction on megathrust stress and slip. *Nature Geoscience*, *13*(3), 249–255. https://doi.org/10.1038/s41561-020-0542-0

Takeuchi, H., Fuji, R., Mimura, N., Imamura, F., Satake, K., Tsuji, Y., et al. (2007). Survey of run-up height of Empo Boso-oki earthquake tsunami on the coast from Chiba prefecture to Fukushima prefecture. *Hist. Earthquake*, *22*, 53–59.

Todd, E. K., Schwartz, S. Y., Mochizuki, K., Wallace, L. M., Sheehan, A. F., Webb, S. C., et al. (2018). Earthquakes and tremor linked to seamount subduction during shallow slow slip at the Hikurangi margin, New Zealand. *Journal of Geophysical Research: Solid Earth*, *123*(8), 6769–6783. https://doi.org/10.1029/2018JB016136

Tozer, B., Sandwell, D. T., Smith, W. H. F., Olson, C., Beale, J. R., & Wessel, P. (2019). Global bathymetry and topography at 15 arc sec: SRTM15+. *Earth and Space Science*, *6*(10), 1847–1864. https://doi.org/10.1029/2019EA000658

Tsuru, T., Park, J.-O., Miura, S., Kodaira, S., Kido, Y., & Hayashi, T. (2002). Along-arc structural variation of the plate boundary at the Japan Trench margin: Implication of interplate coupling. *Journal of Geophysical Research*, *107*(B12), ESE11-1–ESE11-15. https://doi.org/10.1029/2001JB001664

Uchida, N., Nakajima, J., Hasegawa, A., & Matsuzawa, T. (2009). What controls interplate coupling? Evidence for abrupt change in coupling across a border between two overlying plates in the NE Japan subduction zone. *Earth and Planetary Science Letters*, *283*(1), 111–121. https://doi.org/10.1016/j.epsl.2009.04.003

Wallace, L. M., & Beavan, J. (2010). Diverse slow slip behavior at the Hikurangi subduction margin, New Zealand. *Journal of Geophysical Research*, *115*(B12), B12402. https://doi.org/10.1029/2010JB007717

Wallace, L. M., Webb, S. C., Ito, Y., Mochizuki, K., Hino, R., Henrys, S., et al. (2016). Slow slip near the trench at the Hikurangi subduction zone, New Zealand. *Science*, *352*(6286), 701–704. https://doi.org/10.1126/science.aaf2349

Wang, K., & Bilek, S. L. (2011). Do subducting seamounts generate or stop large earthquakes? *Geology*, *39*(9), 819–822. https://doi.org/10.1130/G31856.1

Yamamoto, Y., Takahashi, T., Kaiho, Y., Obana, K., Nakanishi, A., Kodaira, S., & Kaneda, Y. (2017). Seismic structure off the Kii Peninsula, Japan, deduced from passive- and active-source seismographic data. *Earth and Planetary Science Letters*, *461*, 163–175. https://doi.org/10.1016/j.epsl.2017.01.003

Yamaya, L., Mochizuki, K., Akuhara, T., Takemura, S., Shinohara, M., & Yamada, T. (2022). CMT inversion for small-to-moderate earthquakes applying to dense short-period OBS array at off Ibaraki region. *Earth Planets and Space*, *74*(1), 164. https://doi.org/10.1186/s40623-022-01721-3

Yanagisawa, H., Goto, K., Sugawara, D., Kanamaru, K., Iwamoto, N., & Takamori, Y. (2016). Tsunami earthquake can occur elsewhere along the Japan trench—Historical and geological evidence for the 1677 earthquake and tsunami. *Journal of Geophysical Research: Solid Earth*, *121*(5), 3504–3516. https://doi.org/10.1002/2015JB012617

Yokota, Y., Ishikawa, T., Watanabe, S., Tashiro, T., & Asada, A. (2016). Seafloor geodetic constraints on interplate coupling of the Nankai Trough megathrust zone. *Nature*, *534*(7607), 374–377. https://doi.org/10.1038/nature17632